CHEMISTRY
A EUROPEAN JOURNAL

DOI: 10.1002/chem.200801493

Oxidation of Ethers, Alcohols, and Unfunctionalized Hydrocarbons by the Methyltrioxorhenium/H_2O_2 System: A Computational Study on Catalytic C–H Bond Activation

Erik A. Karlsson and Timofei Privalov*[a]

Abstract: The potential-energy surfaces (PESs) of methyltrioxorhenium (MTO)-catalyzed C–H insertion reactions in the presence of hydrogen peroxide were studied by accurate DFT methods for a series of substrates including unsaturated hydrocarbons, an ether, and an alcohol. Based on the comprehensive analysis of transition states and intrinsic reaction coordinate (IRC) scans, C–H insertion was found to proceed by a concerted mechanism that does not require, as previously thought, a side-on or a butterfly-like transition state. We found that a typical transition state follows requirements of the S_N2 reaction instead. Furthermore, by exploring the PESs of several C–H insertion reactions, we discovered that no ionic intermediate is formed even in a polar solvent. The latter was modeled within the self-consistent reaction field approach in a polarizable continuum model (PB-SCRF/PCM). According to our study, C–H insertion occurs by a concerted but highly asynchronous mechanism that first proceeds by hydride transfer and then turns into hydroxide transfer/rebound. For the oxidation of alcohols, C–H bond cleavage occurs without formation of alkoxide intermediates on the dominant pathway. The computed deuterium kinetic isotope effect of 2.9 for the hydride-transfer transition state for alcohol oxidation is in good agreement with the experimental k_H/k_D ration of 3.2 reported by Zauche and Espenson. As confirmed by IRC and PES scans in different solvents, the OH-rebound phase of the C–H insertion pathway demonstrates strong similarities with the rebound mechanism that was previously proposed for cytochrome P450 and metalloporphyrin-catalyzed oxidations.

Keywords: C–H activation · density functional calculations · oxidation · reaction mechanisms · rhenium

Introduction

Combining selective activation of a C–H bond, for example, in an alkane, with subsequent selective functionalization through C–O bond formation is a challenging task.[1–4] Since the first Ru-catalyzed C–H activation reaction reported by Chatt and Davidson[5] and the Pt^{II}-catalyzed activation of primary C–H bonds observed by Shilov and Shul'pin[6,7] in H/D scrambling of alkanes in D_2O/DOAc, it has been firmly established that C–H activation is typically carried out by early transition-metal complexes with d^0 electronic configuration or by late transition metals in low oxidation states, for example, Ir^{I}, Ir^{III}, Ru^{II}, and Os^{II}.[8] The C–O coupling/functionalization step is typically carried out by late transition metal complexes with relatively high oxidation state of the metal center, such as Pd^{II}/Pd^{IV}, Pt^{II}/Pt^{IV}, Au^{III}, and Hg^{II}. A combination of C–H activation and C–O coupling apparently demands a bifunctional catalyst which must meet mutually conflicting requirements. According to the substantial body of evidence gathered, methylrhenium trioxide (CH_3ReO_3, MTO)[9] is one of the more attractive systems for this purpose.[10,4c,11]

Methylrhenium trioxide is a widely used catalyst for various oxygen-transfer reactions which employ hydrogen peroxide (H_2O_2) as terminal oxidant.[12,13] Reaction of MTO with H_2O_2 affords monoperoxo complex **A**, which reacts further to form diperoxo rhenium complex **B** (Scheme 1).[10] In solution, **B** is the most abundant species in the equilibrium. A water molecule coordinates to **B** in a highly labile fashion, as established by NMR spectroscopy.[14] Mono-η^2-peroxo rhenium complex $MeRe(O)_2O_2$ and bis(η^2-peroxo) complex $MeReO(O_2)_2$ (**A** and **B** in Scheme 1, see also Figure 1

[a] E. A. Karlsson, Dr. T. Privalov
Department of Organic Chemistry, Arrhenius Laboratory
Stockholm University, 10691 Stockholm (Sweden)
E-mail: priti@organ.su.se

Supporting information (*XYZ* data for all relevant complexes, gas-phase and solvent reference energies, frequency analysis of transition states) for this article is available on the WWW under http://dx.doi.org/10.1002/chem.200801493.

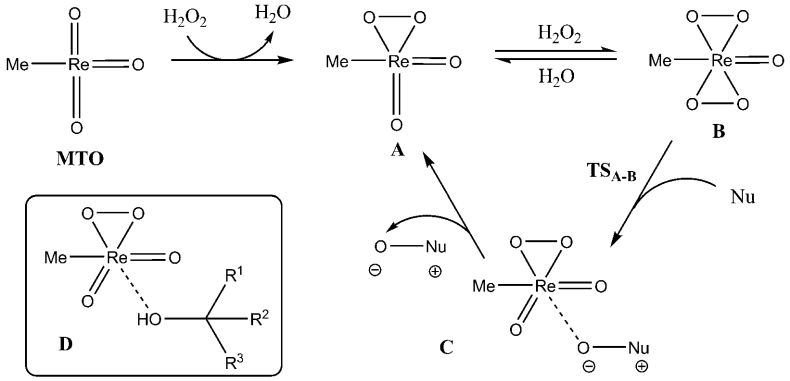

Scheme 1. Generalized mechanism of MTO-catalyzed oxidation (Nu = R_3N, R_3P, R_2S). The inset corresponds to O insertion into a C–H bond of a substrate $C(H)R^1R^2R^3$ without an obvious nucleophilic site.

below), have been fully characterized by X-ray crystallography[15,16] and through their methyl resonances by ^1H and ^{13}C NMR spectroscopy.[17] Employment of hydrogen peroxide as oxygen donor significantly reduces environmental and industrial concerns, and this makes the MTO/H_2O_2 system useful and practical. The solubility of MTO in most organic and aqueous media complements its versatility. Atom-transfer reactions catalyzed by the MTO/H_2O_2 system proceed without free-radical intermediates and without byproducts typically associated with most stoichiometric oxidizing systems.[10] To date MTO combined with various H_2O_2-based terminal oxidants has been used for oxidation of hydrocarbons to alcohols and ketones,[18] olefins to epoxides[19] including pyridine-mediated ligand acceleration,[20] amines to amine oxides, phosphines to phosphine oxides, and sulfides to sulfoxides,[21,22] and for oxidation of alkyl silanes.[11] Methylrhenium trioxide has also been successfully employed in nonvolatile ionic liquids.[23]

The mechanistic essence of a typical MTO-catalyzed oxidation/oxygen transfer is shown in Scheme 1. Unlike other transition metal oxidants the redox reactivity of Re is not involved in the catalytic chemistry of MTO; the Re atom remains in oxidation state VII.[10] Instead it acts as a Lewis acid that activates the peroxide oxygen atoms towards nucleophilic attack. The nucleophile, which could be a heteroatom or the π bond of an olefin, attacks one of the electron-deficient oxygen atoms to form intermediate complex **C**. Dissociative liberation of product from **C** affords monoperoxo Re complex **A**, which is converted back to the active catalyst **B** by reaction with H_2O_2. Relative activity of **A** and **B** depends on the solvent system employed, as reported for the MTO/H_2O_2-catalyzed olefin epoxidation.[24]

Oxidation of unfunctionalized hydrocarbons to alcohols by the MTO/H_2O_2 system[18] is particularly intriguing because, unlike olefins and heteroatom nucleophiles, unfunctionalized hydrocarbons do not have any obvious nucleophilic site that could attack the peroxide oxygen atom in MTO.[25] The reaction does not proceed via radical intermediates either.[26] Based on an analogy with the mechanism of oxidation with dimethyldioxirane (DMDO),[27,28] it was previously suggested that the oxygen atom inserts into the C–H bond via a so-called butterfly transition state[23] with the oxygen approaching from the side of the C–H bond (Scheme 2). However, to the best of our knowledge, there is no direct experimental evidence for the side-on synchronous mechanism. This mechanism is also unlikely due to the great steric hindrance when the C–H bond is approached from the side, especially when R is a tertiary alkyl group (vide infra).

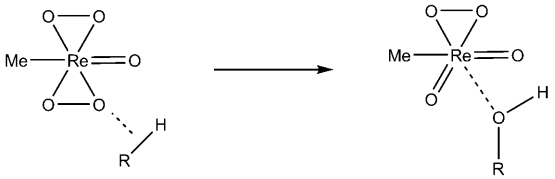

Scheme 2. Synchronous insertion mechanism based on analogy with the mechanism of oxidation with dimethyldioxirane (DMDO).

Herein we propose and investigate an alternative mechanism of oxygen insertion which is initiated by hydride abstraction (Scheme 3) and strongly resembles the so-called oxygen-rebound[29–33] mechanism originally proposed for metalloporphyrin-catalyzed oxidation and cytochrome P450 (vide infra). It is noteworthy that a hydride-abstraction pathway could in theory lead to a carbocationic intermediate, which subsequently collapses to the product. However,

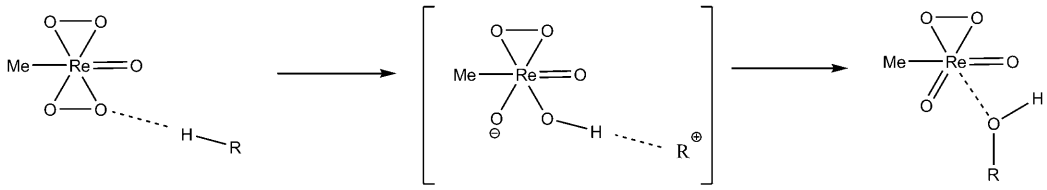

Scheme 3. Hydride abstraction as the activation step of oxygen insertion: if the ionic intermediate is a true stationary point of the multidimensional potential-energy surface the mechanism is stepwise; otherwise, the mechanism has strong similarities to the oxygen-rebound mechanism.

the existence of carbocationic intermediate as a true stationary point of the multidimensional potential energy surface seems to be doubtful. Indeed, 1) rearrangement of a hypothetical ionic intermediate will most probably result in loss of stereochemistry; 2) the hypothetical ion pair could dissociate in a polar solvent and thus liberate the carbocation to react with the solvent. According to experimental data[18] 1) the reaction proceeds with retention of configuration; 2) no ethers resulting from reaction of the carbocation with the alcohol solvent have been detected. The likelihood of the concerted pathway, which resembles oxygen rebound initiated by hydride abstraction, and the likelihood of formation of an intermediate ionic complex will be addressed further.

Considering the importance of MTO/H_2O_2-catalyzed C–H insertion reactions and the apparent uncertainty regarding the mechanism of the reaction, we performed a DFT-based computational study. We show that hydride abstraction and subsequent oxygen rebound describe these C–H insertion reactions very well and are in agreement with available experimental data. Modern DFT methodology is well suited for the elucidation of complex reaction mechanisms. Specifically, our goal was to examine the mechanism of MTO-catalyzed C–H insertion as follows: oxidation of hydrocarbons was modeled for *cis*-1,2-dimethylcyclohexane and toluene; oxidation of ethers and alcohols was modeled for 1-phenylethanol and (1-phenyl)ethyl methyl ether.

Results and Discussion

The catalytically active species are monoperoxo species [$MeRe(O)_2O_2$] (mpRe) and diperoxo complex [$MeReO(O_2)_2$] (dpRe), shown in Figure 1. Our main focus is the activity of dpRe complexes **B′** and **B** with and without the coordinated water molecule (see **B′** and all related transition states in the Supporting Information). As we will show below, monoperoxo complex **A** affords higher potential energy barriers than diperoxo complex **B**, though we are aware that interconversion of **A** and **B** in the presence of H_2O_2/H_2O and specific experimental conditions could greatly influence the relative catalytic activity of mono- and diperoxo complexes. First, "raw" gas-phase potential-energy surfaces (PESs) are discussed, and then solvent effects and full Gibbs free energies.

Oxidation of unfunctionalized hydrocarbons: *cis*-1,2-Dimethylcyclohexane was chosen as a model substrate for the oxidation of unfunctionalized hydrocarbons.[18,34] We first examined the reaction mechanism with diperoxo species [$MeReO(O_2)_2$]. Transition states for insertion into the equatorial and axial C–H bonds were searched for under the assumption that the reaction begins with insertion of an oxygen atom into one of the two tertiary C–H bonds, followed by dissociation of the product (Scheme 4). However, the results (Figure 2) were quite different from what we initially expected. The striking and the unexpected feature of the transition states **TS1** and **TS2** is the linear alignment of the C–H and O– groups, which is more consistent with hydrogen abstraction rather than the expected side-on insertion (see **TS1′** in the Supporting Information). The computational discovery of this linear alignment at the transition state led us to suspect that the reaction starts with hydride abstraction to form the carbocation and the Re-bound OH group, and the latter inserts into the carbocationic center to form the product (**D1** and **D2**, Figure 2).

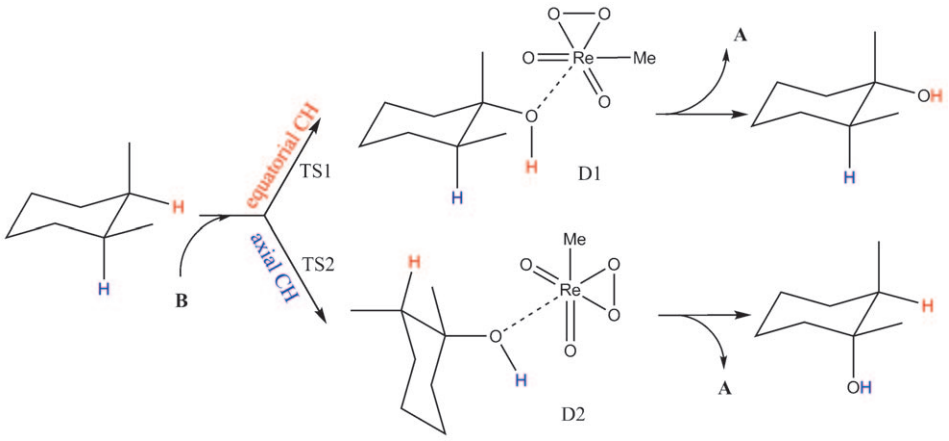

Scheme 4. Oxidation of *cis*-1,2-dimethylcyclohexane by diperoxo complex [$MeReO(O_2)_2$] via insertion into the equatorial and axial C–H bonds. Diperoxo complex [$MeReO(O_2)_2$] is converted to monoperoxo complex [$MeRe(O)_2O_2$].

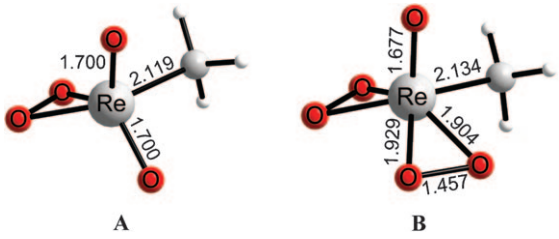

Figure 1. Optimized structure of active monoperoxo complex [$MeRe(O)_2O_2$] (**A**) and the diperoxo complex [$MeReO(O_2)_2$] (**B**). All distances are in angstrom.

Both the equatorial and the axial transition states, **TS1** and **TS2**, have almost equal potential-energy barriers of 23 kcal mol^{-1} with respect to the reference point. The presence of the labile Re-bound water molecule in dpRe complex **B′** affects the corresponding transition-state geometry (**TS1′**, Supporting Information) and slightly raises the potential-energy barrier to 26 kcal mol^{-1}. The reference energy is

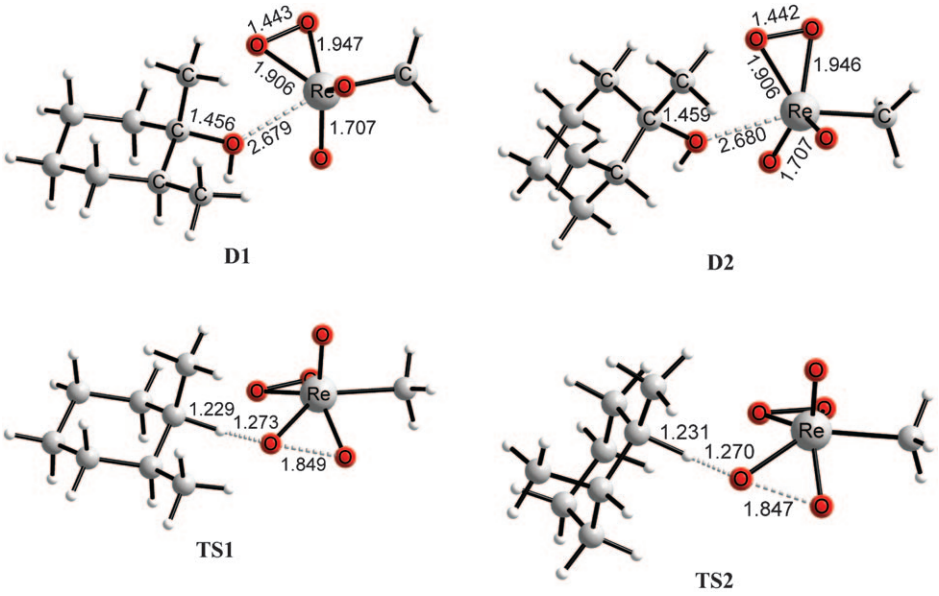

Figure 2. Model without an Re-coordinated water molecule: the transition states for the oxidation of the equatorial and axial C–H bonds of *cis*-1,2-dimethylcyclohexane by [$MeReO(O_2)_2$] (**TS1** and **TS2**, respectively); [$MeRe(O)_2O_2$] complex with Re-bound 1,2-dimethylcyclohexanol product (**D1** and **D2**, respectively). All distances are in angstrom.

the total energy of complex **B** (or **B′**) and *cis*-1,2-dimethylcyclohexane. The increase in the O–O distance in transition state **TS1′** is probably due to the increased planarity of dpRe complex **B′** with an extra Re-bound ligand (see Supporting Information). The former results in much more elongated C–H and much shorter O–H bonds. However, the presence of an extra ligand does not affect the key feature of the transition state: the linear arrangement of the C–H and O–O fragments.

For completeness we located the transition state for oxidation of the equatorial C–H bond by monoperoxo species [$MeRe(O)_2O_2$] (Figure 3): the potential-energy barrier for the monoperoxo transition state is higher than that of the dpRe transition state, by almost 10 kcal mol^{-1}.

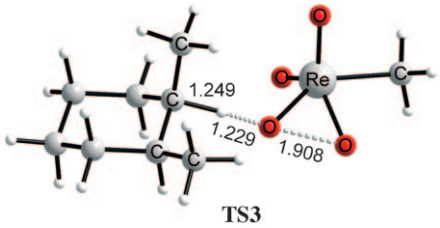

Figure 3. Transition state for oxidation of the equatorial C–H bond of *cis*-1,2-dimethylcyclohexane by monoperoxo complex [$MeRe(O)_2O_2$]. All distances are in angstrom.

To gain further insight into the reaction mechanism, and to find out whether the linear C–H···O–O geometrical motif could be found in the transition states for other substrates, oxidation of toluene and 1-phenylethyl methyl ether by dpRe was modeled. Transition states for hydrogen abstraction were found (Figure 4) for both test cases. Both transition states have a distinctively linear alignment of the C–H and O–O groups, but the potential energy barriers associated with **TS4** and **TS5** are somewhat different: 27 and 21 kcal mol^{-1} respectively. As confirmed by IRC scans (vide infra), hydride abstraction from toluene is followed by the interaction of the OH group with the carbocation of the substrate to form the benzyl alcohol (cf. Schemes 1 and 4), while elimination of MeOH from the O atom hemiacetal insertion intermediate of the ether leads to formation of the ketone acetophenone (Scheme 5). This "rebound" of

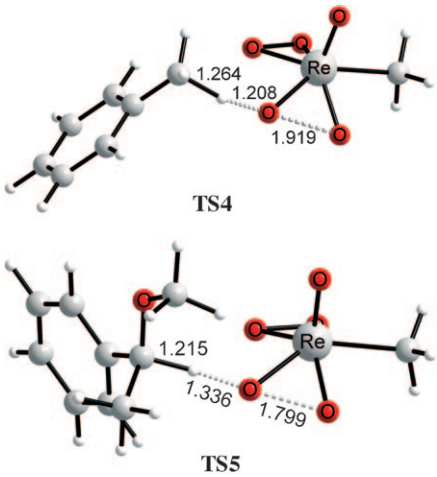

Figure 4. Transition states for oxidation of toluene (**TS4**) and 1-phenylethyl methyl ether (**TS5**, see also Scheme 5) by diperoxo complex [$MeReO(O_2)_2$] in the model without a Re-coordinated water molecule.[43] All distances are in angstrom.

the OH group strongly resembles the oxygen rebound[29–33] originally proposed for metalloporphyrin-catalyzed oxidations and cytochrome P450.

Among all reported transition states within the simplified model that do not include the Re-bound water molecule, the transition state of toluene oxidation **TS4** has the shortest O–H bond and the longest, nearly completely cleaved, O–O bond. Toluene is a much less bulky substrate than 1,2-dimethylcyclohexane, yet all attempts to find any other but the linear transition states failed. Remarkably, the effect of the methoxyl group on the corresponding transition state of an

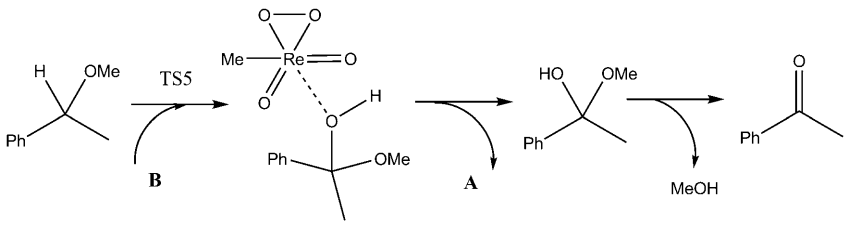

Scheme 5. Oxidation of 1-phenylethyl methyl ether by diperoxo complex [$MeReO(O_2)_2$].

ether complex, **TS5**, resulted in a somewhat larger O–H distance and a shorter O–O distance relative to toluene (Figure 4); nevertheless, transition states for hydrogen abstraction from toluene and the ether are quite similar in terms of both structure and activation energy.

Oxidation of an alcohol by the C–H insertion pathway: We found a "linear" transition state for oxidation of alcohols by complexes **B** and **A**. Attempts to follow the classical mechanism of an alcohol oxidation involving an alkoxide formation with subsequent α-C–H bond cleavage of an alkoxide, as occurs with Pd^{II},[35,36] CrO_3, and vanadium oxide catalysts,[37] were totally unsuccessful. Although it was possible to computationally characterize both the Re alkoxide and the Re carbonyl intermediates, their relative energies were found to be higher than the reference point, the total energy of **B** and 1-phenylethanol, by +10 and +18 kcal mol^{-1}, respectively. The potential-energy barriers on the pathway to the Re alkoxide complex was found to be 24 kcal mol^{-1}, while the potential energy barrier that separates Re alkoxide and Re carbonyl intermediates was found to be almost 40 kcal mol^{-1}. The classical alcohol oxidation reaction pathway involves a change in the oxidation state of the transition metal, for example, Pd^{II}-catalyzed oxidation of alcohols proceeds via a Pd^0 intermediate. It seems that lowering of the oxidation state of Re in the analogous mechanism that proceeds via formation of a Re alkoxide intermediate followed by the Re carbonyl complex is strongly disfavored, which is the reason why we obtained such an unfavorable potential-energy profile.

The only meaningful mechanism that we were able to characterize both with the accurate QST-guided transition search, which afforded **TS6** (Figure 5), and with the IRC scan proceeds in complete analogy with all previously considered cases via hydride abstraction. The potential-energy

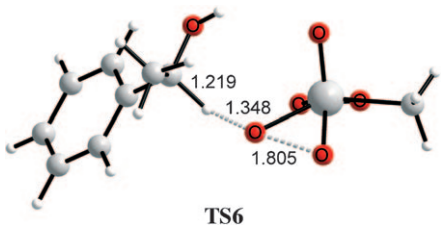

Figure 5. Transition state for oxidation of 1-penylethanol within the model complexes **B**. All distances are in angstrom.

barrier for the formation of acetophenone hydrate is almost 20 kcal mol^{-1} (see discussion of IRC scans below). The hydrate intermediate evolves into the ketone by elimination of a water molecule. It is noteworthy that the hydride-abstraction pathway with subsequent rebound of the OH group does not require a change in the oxidation state of the metal. This pathway is in complete analogy with the oxidation of ethers, as shown in Scheme 5.

According to experimental data,[26] about 80% of the ^{18}O-labeled oxygen atom of the *sec*-phenethyl alcohol remained in the ketone (the MTO/urea·H_2O_2 system was used in these experiments to minimize oxygen exchange between the ketone and solvent). When aqueous H_2O_2 was used, significant exchange of the labeled ketone with solvent oxygen atoms occurred. Our mechanism, which is based on OH rebound triggered by hydride abstraction, gives 50% retention of labeled oxygen. A plausible competing pathway which could account for the discrepancy in retention of the ^{18}O label could involve proton loss, most likely after hydride transfer. The hypothetical mechanism with proton loss should give 100% retention of the labeled oxygen atom. Since the experimentally reported retention is only about 80% and since our mechanism already gives 50% retention, we conclude that the plausible proton loss occurs in a minor competing pathway.

Furthermore, the computed deuterium kinetic isotope effect for **TS6** of 2.9 is in good agreement with the experimental k_H/k_D ratio of 3.2.[26] Therefore, the transition state **TS6** for hydride transfer appears to be consistent with the experimental data reported by Zauche and Espenson.

Solvent effects and molecular orbital analysis: All aforementioned raw potential-energy barriers were obtained in the gas phase. The most straightforward way to account for solvent effects is to employ a self-consistent reaction field in a polarizable continuum solvent model (PB-SCRF/PCM).[38]

Solvent effects adjust the gas-phase data to only a small extent (see Table 1) in the case of the aforementioned transition states. Even in the most polar solvent considered, water, solvent effects are less that 4 kcal mol^{-1}. The absence of a dramatic stabilization of a linear transition state even in a highly polar solvent does not speak in favor of formation of an ionic intermediate (see discussion below). Full Gibbs free-energy data including all thermochemical corrections to the raw potential energy in the gas phase are reported in Table 1.

In all considered C–H insertion reactions, frontier orbital interactions of a substrate and the active catalytic complex are closely reminiscent of the frontier orbital interactions used to describe the S_N2 reaction. According to the established mechanism of the S_N2 reaction, so-called backside attack enables the necessary frontier orbital overlap. A side

Table 1. Computed barriers in the gas phase and in solvent (toluene, methanol, and water) in the model without Re-bound water molecule (**B**). Calculated $\Delta G^{\ddagger}$ [reported in brackets] are based on full Gibbs free energy in the gas phase; $\Delta E^{\ddagger}$ are computed on the basis of raw potential energies. All computations were performed with respect to the reference point, which is the total electronic/Gibbs free energy of **B** and the corresponding substrate.

	$\Delta E^{\ddagger}$ (gas phase) [$\Delta G^{\ddagger}$ (gas phase)]	$\Delta E^{\ddagger}$ (toluene)	$\Delta E^{\ddagger}$ (MeCN)	$\Delta E^{\ddagger}$ (H_2O)
TS1	22.7 [33.1]	21.9	21.4	20.2
TS2	23.0 [33.4]	22.3	22.1	21.0
TS3	29.9 [38.4]	29.2	28.6	27.9
TS4	26.7 [37.4]	26.1	24.9	23.1
TS5	20.7 [32.1]	20.6	22.4	20.0
TS6	19.8 [29.9]	21.7	23.2	22.3

attack has several disadvantages, of which poor frontier orbital overlap is the major one and is accompanied by substantial steric hindrance, which explains why no side-on transition states were found. A linearly aligned transition state has much less steric hindrance than synchronous side-on insertion. Mulliken population analysis is consistent with formation of the carbocation transition state in all cases.

Evolution of a reacting complex along the intrinsic reaction coordinate: All reported transition states clearly point in the direction of hydride abstraction in the initial reaction step with almost linear arrangement of C–H and O–O parts. The key question is what happens after the linearly aligned transition state. To investigate this further a series of intrinsic reaction coordinate (IRC) scans was performed mapping the PES along the reaction coordinate from the transition state towards the product in the model with and without Re-bound water molecule. The IRC scans were performed for all model reactions and almost identical PESs were obtained. Selected structures (optimized snapshots along the reaction coordinate) from a typical IRC scan are shown in Figure 6 (all energies in Figure 6 are relative raw potential energies with respect to the total energy of complex **B** and *cis*-1,2-dimethylcyclohexane).

The IRC scan reveals that the reaction proceeds from the transition state to the product complex in a concerted fashion without any additional intermediates. The evolution can be qualitatively broken down into three distinct stages: 1) hydride transfer to the Re-bound oxygen atom, whereby population of the O–O antibonding orbital like in a classical S_N2 reaction leads to apparent cleavage of the O–O bond; 2) rotation of the OH group around the Re–O bond reorients the dipole with respect to the carbocation while retaining distinctive Re–O bonding; 3) the OH group rebinds to the carbocation. Relaxing the geometries of all reported transition states and IRC scan frames, both in the relatively unpolar solvent toluene and in the highly polar protic solvent water, directly afforded the product complexes in all cases. Thus, our exploration of the potential surface along the reaction coordinate proves that hydride transfer and the subsequent hydroxide transfer/rebound occur in a concerted but highly asynchronous fashion. This mechanism shares some strong similarities with the aforementioned oxygen-rebound mechanism proposed for cytochrome P450 and metalloporphyrin-catalyzed oxidation,[29–33] though the latter is usually considered to be a stepwise process.

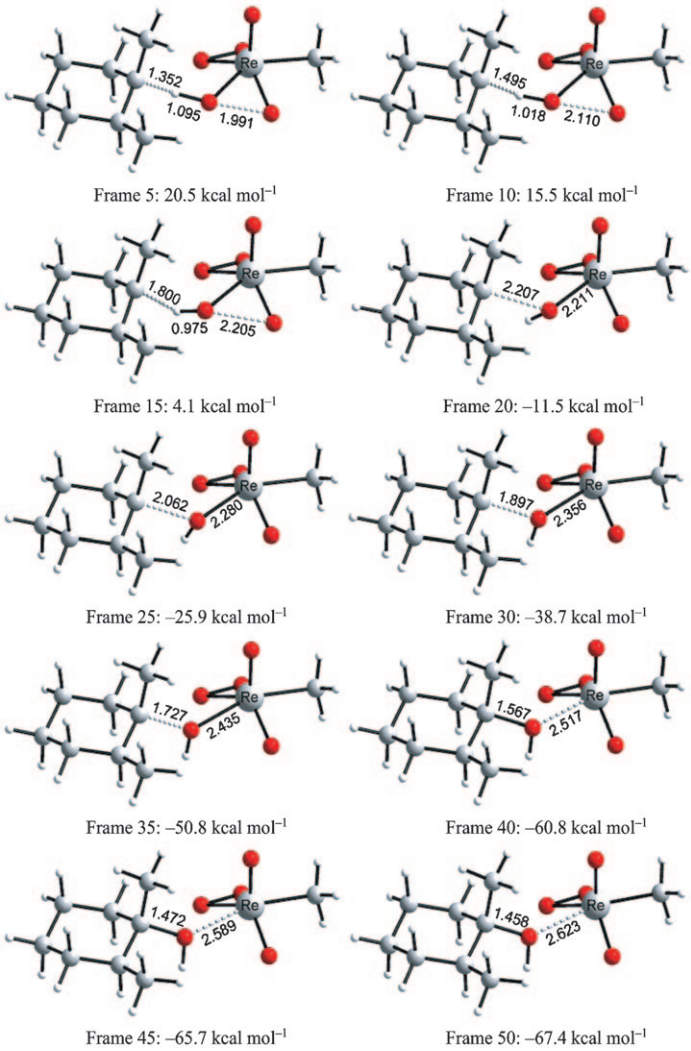

Figure 6. Selected frames from IRC scan from transition state **TS1** towards **D1**. All distances are in angstrom. All energies are in kcal mol^{-1}. OH rebound is clearly seen starting from Frame 30 onwards.

Conclusion

The reaction of MTO/H_2O_2 with substrates such as *cis*-1,2-dimethylcyclohexane, toluene, 1-phenylethanol, and 1-phenylethyl methyl ether has been studied by density functional computations.

Starting with the unfunctionalized hydrocarbons *cis*-1,2-dimethylcyclohexane and toluene, our initial idea was that C–H cleavage and O insertion could proceed via two competing reaction pathways involving a plausible linear and a side-on (or butterfly-type) transition state. However, attempts to find a transition state for side-on insertion were

systematically unsuccessful. We computationally discovered that the interaction between the C–H group of the substrate and the O–O group of dpRe and mpRe is facilitated by the linear alignment. Based on the analysis of frontier orbital interactions and effects of steric congestion we conclude that S_N2-like requirements apply to the transition state found not only for unfunctionalized hydrocarbons, but also for 1-phenylethyl methyl ether and 1-phenylethanol.

The relatively small size of the complete computational models, which include monoperoxo complex [$MeRe(O)_2O_2$] or diperoxo complex [$MeReO(O_2)_2$] together with a substrate, allowed thorough exploration of the potential-energy surface. The S_N2-like hydride-transfer step triggers OH rebound to the carbocation, which resembles the rebound mechanism proposed for cytochrome P450 and related metalloporphyrin-catalyzed oxidations. Based on the comprehensive computational profiling of potential-energy surfaces, we conclude that no ionic intermediate is formed.

Furthermore, the C–H insertion mechanism based on hydride transfer and OH rebound provides a much more reasonable activation energy for the oxidation of alcohols by MTO/H_2O_2 than the classical oxidation mechanism, which proceeds via metal alkoxide and metal carbonyl intermediates. Accurate IRC scans of the potential-energy surface describing alcohol oxidation support the concerted C–H insertion mechanism analogous to that of unfunctionalized hydrocarbons. The computed deuterium kinetic isotope effect for the transition state of the hydride transfer is in good agreement with the experimental data, though lower retention of the ^{18}O label indicates the presence of a minor competing pathway. While our computational/mechanistic discovery of an unusual C–H insertion pathway for alcohols may require some additional experimental support, we argue that the monoperoxo complex [$MeRe(O)_2O_2$] and diperoxo complex [$MeReO(O_2)_2$] afford only unstable intermediates with alkoxide and carbonyl moieties along the traditional alcohol oxidation pathway.

Computational Procedures

Gas-phase geometry optimizations of all intermediates and transition states were performed by using the B3LYP functional[39] and lacvp**/6-31G(d,p) basis set[40,41] with the model formally in the gas phase. All degrees of freedom were optimized. The transition states were characterized by a single imaginary vibrational frequency along the reaction coordinate. All gas-phase computations were performed with Jaguar v. 4.0 and v. 6.0; computation of all transition states, all intrinsic reaction coordinate (IRC) scans, and PB-SCRF calculations were performed with Jaguar v. 6.0.[42] Vibrational frequencies and full Gibbs free energies were computed in Jaguar 6.0 with the B3LYP density functional at the lacvp**/6-31G(d,p) basis-set level.

Gas-phase optimized transition-state structures were used as initial guesses in solvent calculations within the PB-SCRF. Geometry optimizations of intermediates were performed using PB-SCRF in an attempt to locate plausible ionic intermediates and to verify results of IRC scans. All potential-energy profiling was performed along the intrinsic reaction coordinate as defined by the Hessian of the corresponding transition state. Potential-energy profiling was performed with and without the labile Rebound water molecule with essentially identical outcome. The reference point for all calculations of raw potential-energy barriers and full relative Gibbs free energies is the total energy of an appropriate substrate and complex **A**, **B**, or **B′**.

Acknowledgements

We acknowledge the Swedish Research Council and K&A Wallenberg Foundation for financial support of this work. Prof. Jan-E. Bäckvall and Prof. H. Adolfsson are acknowledged for fruitful discussions.

[1] R. H. Crabtree, *Chem. Rev.* **1995**, *95*, 987.
[2] A. E. Shilov, G. B. Shul′pin, *Chem. Rev.* **1997**, *97*, 2879.
[3] T. Strassner, M. Muehlhofer, A. Zeller, E. Herdtweck, W. A. Herrmann, *J. Organomet. Chem.* **2004**, *689*, 1418.
[4] a) J. Kua, X. Xu, R. A. Periana, W. A. Goddard III, *Organometallics* **2002**, *21*, 511; b) X. Xu, J. Kua, R. A. Periana, W. A. Goddard III, *Organometallics* **2003**, *22*, 2057; c) J. M. Gonzales, R. Distasio, Jr., R. A. Periana, W. A. Goddard III, *J. Am. Chem. Soc.* **2007**, *129*, 15794.
[5] J. Chatt, J. M. Davidson, *J. Chem. Soc.* **1965**, 843.
[6] A. E. Shilov, G. B. Shul′pin, *Activation and Catalytic Reactions of Saturated Hydrocarbons*, Kluwer, Dordrecht, **2000**.
[7] R. H. Crabtree, *J. Chem. Soc. Dalton Trans.* **2001**, 2437.
[8] R. H. Crabtree, *The Organometallic Chemistry of the Transition Metals*, 4th ed., Wiley, New York, **2005**, p. 364.
[9] a) W. A. Herman, R. W. Fisher, D. W. Marz, *Chem. Rev.* **1997**, *97*, 3197; b) I. R. Beattie, P. J. Jones, *Inorg. Chem.* **1979**, *18*, 2318; c) See also review by: H. Adolfsson, D. Balan in *Aziridines and Epoxides in Organic Synthesis* (Ed.: A. K. Yudin), Wiley, New York, **2006**, p. 211.
[10] J. H. Espenson, *Chem. Commun.* **1999**, 479.
[11] H. Tan, A. Yoshikawa, M. S. Gordon, J. H. Espenson, *Organometallics* **1999**, *18*, 4753.
[12] G. Bianchini, M. Crucianelli, C. Canevali, C. Crestini, F. Morazzoni, R. Saladino, *Tetrahedron* **2006**, *62*, 12326.
[13] M. Johansson, A. A. Linden, J.-E. Bäckvall, *J. Organomet. Chem.* **2005**, *690*, 3614.
[14] See discussion in reference [9c].
[15] W. A. Herrmann, R. W. Fisher, W. Scherer, M. U. Rauch, *Angew. Chem.* **1993**, *105*, 1209; *Angew. Chem. Int. Ed. Engl.* **1993**, *32*, 1157.
[16] S. Yamazaki, J. H. Espenson, P. Huston, *Inorg. Chem.* **1993**, *32*, 4683.
[17] M. M. Abu-Omar, P. J. Hansen, J. H. Espenson, *J. Am. Chem. Soc.* **1996**, *118*, 4966.
[18] R. W. Murray, K. Iyanar, J. Chen, J. T. Wearing, *Tetrahedron Lett.* **1995**, *36*, 6415.
[19] a) F. E. Kuhl, W. A. Herrmann, *Chemtracts: Org. Chem.* **2001**, *14*, 59; b) W. A. Herrmann, R. W. Ficher, D. W. Marz, *Angew. Chem.* **1991**, *103*, 1706; *Angew. Chem. Int. Ed. Engl.* **1991**, *30*, 1638; c) W. A. Herrmann, R. W. Ficher, M. U. Rauch, W. Scherer, *J. Mol. Catal.* **1994**, *86*, 243; d) W. Adam, C. M. Mitchell, *Angew. Chem.* **1996**, *108*, 578; *Angew. Chem. Int. Ed. Engl.* **1996**, *35*, 533.
[20] J. Rudolph, K. L. Reddy, J. P. Chiang, K. B. Sharpless, *J. Am. Chem. Soc.* **1997**, *119*, 6189.
[21] a) S. Yamazaki, *Org. Biomol. Chem.* **2007**, *5*, 2109; b) G. B. Sul′pin, *C. R. Chim.* **2003**, *6*, 163; c) G. V. Nizova, C. Bolm, S. Ceccarelli, C. Pavan, G. B. Shul′pin, *Adv. Synth. Catal.* **2002**, *344*, 899; d) U. Schuchardt, D. Mandelli, G. B. Shul′pin, *Tetrahedron Lett.* **1996**, *37*, 6487.
[22] General reviews about MTO catalysis: a) F. E. Kuhl, A. Scherbaum, W. A. Herrmann, *J. Organomet. Chem.* **2004**, *689*, 4149; b) G. S. Owens, J. Arias, M. M. Abu-Omar, *Catal. Today* **2000**, *55*, 317; c) K. P. Gable, *Adv. Organomet. Chem.* **1997**, *41*, 127.
[23] a) G. S. Owens, M. M. Abu-Omar, *Chem. Commun.* **2000**, 1165; b) G. Bianchini, M. Crucianelli, F. De Angelis, V. Neri, R. Saladino, *Tetrahedron Lett.* **2005**, *46*, 2427.
[24] G. S. Owens, A. Durazzo, M. M. Abu-Omar, *Chem. Eur. J.* **2002**, *8*, 3053.

[25] If the substrate is a hydrocarbon the product alcohol is produced directly. If the substrate is a secondary alcohol a carbonyl hydrate is produced, which then eliminates water to form the ketone.
[26] T. H. Zauche, J. H. Espenson, *Inorg. Chem.* **1998**, *37*, 6827.
[27] R. W. Murray, R. Jeyaraman, L. Mohan, *J. Am. Chem. Soc.* **1986**, *108*, 2470.
[28] R. Mello, M. Fiorentino, C. Fusco, R. Curci, *J. Am. Chem. Soc.* **1989**, *111*, 6749.
[29] a) M. Filatov, S. Shaik, *J. Phys. Chem. A* **1998**, *102*, 3835; b) F. Ogliaro, N. Harris, S. Cohen, M. Filatov, S. P. de Visser, S. Shaik, *J. Am. Chem. Soc.* **2000**, *122*, 8977;
[30] P. E. M. Siegbahn, *J. Biol. Inorg. Chem.* **2001**, *6*, 27.
[31] H. Basch, K. Mogi, D. G. Musaev, K. Morokuma, *J. Phys. Chem. A* **2001**, *105*, 3615.
[32] a) J. T. Groves, *J. Chem. Educ.* **1985**, *62*, 928; b) J. T. Groves, *J. Porphyrins Phthalocyanines* **2000**, *4*, 350.
[33] D. Balcells, C. Raynaud, R. H. Crabtree, O. Eisenstein, *Chem. Commun.* **2008**, 744.
[34] G. Bianchini, M. Crucianelli, C. Canevali, C. Crestini, F. Morazzoni, R. Saladino, *Tetrahedron* **2006**, *62*, 12326.
[35] For reviews and excellent references, see: a) R. A. Sheldon, I. W. C. E. Arends, A. Dijksman, *Catal. Today* **2000**, *57*, 157; b) R. A. Sheldon, I. W. C. E. Arends, G.-J. ten Brink, A. Dijksman, *Acc. Chem. Res.* **2002**, *35*, 774; c) J. Muzart, *Tetrahedron* **2003**, *59*, 5789; d) S. S. Stahl, *Angew. Chem.* **2004**, *116*, 3480; *Angew. Chem. Int. Ed.* **2004**, *43*, 3400; e) T. Nishimura, K. Ohe, S. Uemura, *Synlett* **2004**, 201.
[36] a) S. Paavola, K. Zetterberg, T. Privalov, I. Csöregh, C. Moberg, *Adv. Synth. Catal.* **2004**, *346*, 237; b) T. Privalov, C. Linde, Z. Zetterberg, C. Moberg, *Organometallics* **2004**, *23*, 885; c) M. Schultz, R. Adler, W. Zierkiewicz, T. Privalov, M. Sigman, *J. Am. Chem. Soc.* **2005**, *127*, 8499.
[37] J. Döbler, M. Pritzsche, J. Sauer, *J. Am. Chem. Soc.* **2005**, *127*, 10861.
[38] Jaguar 6.0 package treats solvated molecular systems with PB-SCRF method by using its own Poisson–Boltzmann solver, which makes it possible to compute solvation energies and minimum-energy solvated structures of solvated transition states. For details, see: a) D. J. Tannor, B. Marten, R. Murphy, R. A. Friesner, D. Sitkoff, A. Nicholls, M. Ringnalda, W. A. Goddard III, B. Honig, *J. Am. Chem. Soc.* **1994**, *116*, 11875; b) B. Marten, K. Kim, C. Cortis, R. A. Friesner, R. B. Murphy, M. N. Ringnalda, D. Sitkoff, B. Honig, *J. Phys. Chem.* **1996**, *100*, 11775; c) C. J. Cramer, G. D. Truhlar, *Chem. Rev.* **1999**, *99*, 2161.
[39] a) A. D. Becke, *J. Chem. Phys.* **1993**, *98*, 5648; b) C. Lee, W. Yang, R. G. Parr, *Phys. Rev. B* **1988**, *37*, 785.
[40] P. J. Hay, W. R. Wadt, *J. Chem. Phys.* **1985**, *82*, 299.
[41] a) W. J. Hehre, R. Ditchfield, J. A. Pople, *J. Chem. Phys.* **1972**, *56*, 2257; b) M. M. Francl, W. J. Pietro, W. J. Hehre, J. S. Binkley, M. S. Gordon, D. J. Defrees, J. A. Pople, *J. Chem. Phys.* **1982**, *77*, 3654; c) P. C. Hariharan, J. A. Pople, *Theor. Chim. Acta* **1973**, *28*, 213.
[42] Jaguar versions 4.0 and 6.0, Schrödinger, Portland, OR, **1991–2000**.
[43] The addition of the Re-bound water molecule did not affect **TS4** and **TS5** to any significant extent. The presence of a labile Re-bound ligand complicates convergence during the transition search and IRC scans because of the presence of several nearly degenerate local minimum configurations and the lack of the direct ligand–solvent interactions. To reduce the associated computational uncertainty, we performed the majority of our study both with and without the labile Re-bound water molecule.

Received: July 23, 2008
Revised: November 13, 2008
Published online: January 8, 2009

